Modeling a Spin-Labeled Fusion Peptide in a Membrane: Implications for the Interpretation of EPR Experiments

Maria Sammalkorpi*† and Themis Lazaridis†
*Mechanical and Aerospace Engineering, Princeton University, Princeton, New Jersey; and †Department of Chemistry, City College of the City University of New York, New York

ABSTRACT Site-directed spin-labeling and electron paramagnetic resonance are powerful tools for studying structure and conformational dynamics of proteins, especially in membranes. The position of the spin label is used as an indicator of the position of the site to which it is attached. The interpretation of these experiments is based on the assumptions that the spin label does not affect the peptide configuration and that it has a fixed orientation and distance with respect to the protein backbone. Here, the validity of these assumptions is examined through implicit membrane molecular dynamics simulations of the influenza hemagglutinin fusion peptide that has been labeled with methanethiosulfonate spin label. We find that the methanethiosulfonate spin label can occasionally induce peptide orientations that differ from those adopted by the wild-type peptide. Furthermore, the spin-label resides, on average, several Ångstroms deeper in the membrane than the corresponding backbone C_α-atom even at sites pointing toward the solvent. The nitroxide spin label exhibits flexibility and adopts various configurations depending on the surrounding residues.

INTRODUCTION

Site-directed spin-labeling combined with electron paramagnetic resonance (EPR) is a commonly used and powerful tool for measurements of structure and conformational dynamics of both soluble and membrane proteins (1–8). The method involves a site-specific cysteine mutation, which is typically labeled with a nitroxide spin label. EPR measurements of the spectral properties of the paramagnetic unpaired electron in this spin label provide information about the environment, such as membrane insertion depth, mobility of the spin label, polarity of the environment, and distance to another paramagnetic subgroup in the system (5–9). EPR has been used for studying protein conformational changes through distance measurements between two paramagnetic electrons in a system (10–13), as well as for prediction of backbone dynamics (14,15) and to study the membrane insertion depth of a protein or a peptide and its secondary structure (13,16–19).

The analysis of EPR data in membrane systems is usually based on the assumption that the spin label adopts a fixed orientation and distance with respect to the backbone. However, most spin-label residues are not immobilized by the surroundings; in fact, the EPR measurements convey information about both backbone dynamics and spin-label dynamics (4). Furthermore, crystal structures showed that the spin label may adopt a variety of orientations and conformations with respect to the backbone (20). A recent study addressed the flexibility issue by combining modeling of the spin-label orientation and measurements (21), and another one utilized molecular dynamics simulations to determine preferred labeling sites (22), but this is rare. The assumptions of fixed orientation and distance from the backbone become especially significant when the data is employed to predict secondary structure and insertion depth of a membrane protein. Site-dependent spin-label configurations could emerge with greater likelihood at surface sites and in the presence of a hydrophobicity gradient, such as at the lipid bilayer-water interface.

In Macosco et al. (17) and Han et al. (23), site-specific mutations and EPR were used to obtain a spin-label insertion depth profile (24) for the hemagglutinin fusion peptide. The profile was employed in deducing the membrane insertion depth and orientation of the labeled peptide with the help of the assumption that the distance and configuration of the spin label with respect to the peptide backbone are the same for all the labeled residues (17,23). Based on methanethiosulfonate spin-label (MTSSL) measurements, Macosco et al. (17) predicted an α-helix with a membrane insertion angle of 25° and membrane insertion depth somewhat deeper than the lipid phosphate group. Han et al. introduced a hydrophilic extension tail to the peptide and deduced that the peptide adopts a V-shaped helix-break-helix configuration that has both the N- and the C-termini inserted into the membrane (23). Other studies of the hemagglutinin fusion peptide reported a helical structure with 45° tilt angle (25), N-terminus insertion depth close to phosphate headgroup (26), and an orientation along the membrane-water interface for a glutamic-acid-rich analog (27).

The MTSSL is a relatively long and flexible residue (20,28) and has been demonstrated to adopt several site-dependent conformations in crystal structures (20). In addition, the label is more hydrophobic than the majority of the residues it replaces (29), and may affect the membrane insertion depth. In this work, we employ molecular dynamics simulations of the well-studied influenza hemagglutinin

Submitted July 5, 2006, and accepted for publication September 12, 2006.

Address reprint requests to T. Lazaridis, E-mail: tlazaridis@sci.ccny.cuny.edu.

M. Sammalkorpi was formerly M. Huhtala.

0006-3495/07/01/10/13 $2.00

doi: 10.1529/biophysj.106.092809

fusion peptide, i.e., a 20-residue-long N-terminal sequence of influenza hemagglutinin, as a test platform for studying the configurational variety of the MTSSL. The spin label is presented in Fig. 1. The influenza hemagglutinin fusion peptide was chosen because there are two independent MTSSL-based studies of membrane orientation of this peptide (17,23) and also because we (30), and others (31–33), have been unable to reproduce the proposed orientation based on the EPR studies. Our simulations predict the peptide to adopt a slightly tilted orientation along the lipid headgroup-tail interface (30), whereas Bechor and Ben-Tal (32) predicts an interfacial orientation, Efremov et al. (31) report an angle between 10.3 and 18.0° but an insertion depth of only 1.4 Å into the lipid headgroup region, and Spassov et al. (33) report the peptide to reside in the interface at an angle of 20–25° but only if one helix turn at the N-terminus unwraps—for intact helix, the orientation was practically parallel to the membrane-water interface. We model the site-specific MTSSL mutations of Macosco et al. (17) and Han et al. (23) and study by molecular dynamics simulations the configurations of the mutant peptide and the spin label in the membrane. The results suggest that the configurational flexibility of the spin-label residue should be taken into account in EPR data analysis.

COMPUTATIONAL METHODS

In Macosco et al. (17), the following mutations were studied: A5C, I6C, A7C, G8C, I10C, N12C, G13C, and W14C. Here, *C* refers to the MTSSL-labeled cysteine residue (see Fig. 1). Han et al. introduced an additional hydrophilic seven-residue tail to the fusion peptide in their study (23). Mutations to all except G4 and G8 in the 20-residue fusion peptide sequence were studied. We reproduce, one by one, the mutations of Macosco et al. (17) in a 20-residue-long hemagglutinin fusion peptide sequence of influenza strain X31 (GLFGAIAGFI**E**NGW**E**GMI**D**G), and the mutations of Han et al. (23) in the extended 27-residue sequence that adds the artificial tail (-GCGKKKK) to the aforementioned sequence. The acidic residues (underlined) are either deprotonated (charged) or protonated (neutral), and in the simulations of the extended 27-residue peptide, the native cysteine in the tail has been replaced by a serine in accord with the experiments (23).

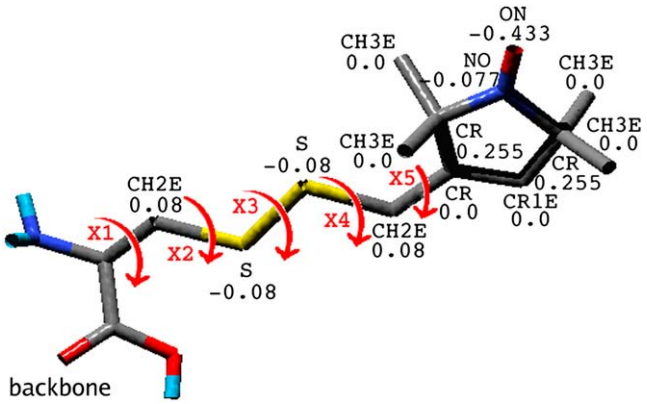

FIGURE 1 The methanethiosulfonate spin label (MTSSL) attached to cysteine. The symbols next to the atoms refer to the atom type and partial charge used in CHARMM. The angles χ_1–χ_5 refer to dihedral angles in the residue. We employ the CHARMM 19 force field (35) that treats nonpolar hydrogens implicitly.

The CHARMM 19 force field that treats nonpolar hydrogen atoms implicitly is employed to describe the intramolecular interactions in the peptide (34,35). The EFF1.1 implicit description of water and the IMM1 description of the membrane are used to describe the environment (36,37). The hydrophobic thickness T of the bilayer depends on the type of lipids and typically ranges between 20 Å and 30 Å. A value of $T = 26$ Å has been used in this work. The CHARMM 19 force field (35) and the IMM1 solvation model (36) do not include parameters for the nitroxyl label. The parameterization is presented in Appendix A.

We start by sampling the membrane configurations of the spin-labeled influenza hemagglutinin fusion peptide. The peptide is placed close to, or into the membrane, as an initially ideal, obliquely inserted α-helix. The initial insertion angle ranges between 0 and 90° with respect to the membrane at intervals of 15°. Two insertion depths are tried: center of mass initially at $z =$ 0.0 Å (at the center of membrane) or at $z = 13.0$ Å (at the polar-nonpolar interface). The initial structure is allowed to evolve freely for 500 ps at 300 K, after which the system is minimized for 300 steps by the adopted basis Newton-Raphson method (34) to obtain comparable initial configurations. The use of an implicit environment description provides significantly faster relaxation than all-atom molecular dynamics simulations. The obtained relaxed configurations are then simulated for 500 ps by employing the Nosé-Hoover thermostat with heat bath coupling constant $q = 100$ (38,39). The trajectory of the last 400 ps of this part of the simulation is used to characterize the membrane orientation, insertion, and energetics of the peptide.

For each site-labeled mutant, the configuration that corresponds to the most typical run of the ensemble resulting from the above runs of a particular mutant is selected and subjected to a 5-ns Nosé-Hoover simulation. This trajectory is employed to calculate the average membrane insertion depths and orientations of the spin label and the dihedral angle distributions of the spin label. The orientations, insertion depths, and dihedral angle distributions are averaged over simulation frames sampled every 500 steps.

In the simulations, the N-terminus is deprotonated while the acidic residues are protonated or deprotonated. The effective energy values presented do not include the cost of (de)protonation and the entropic contributions to the free energy. Therefore, the effective energy values are comparable only within a given state.

RESULTS

The wild-type HA fusion peptide monomer adopts in the simulations a slightly tilted orientation along the lipid headgroup-tail interface (Fig. 2). The adopted angle ranges between 5 and 25° with an average of 12.4 ± 4.2° and the insertion depth corresponds to the N-terminus residing at the lipid headgroup-tail interface (30).

In the simulations of the spin-labeled peptides, the orientation and the position of the mutated peptide in the membrane as well as the depth of the nitroxide spin label in the membrane are monitored for each of the studied mutants. The simulated peptides adopt the slightly tilted interfacial orientation depicted in Fig. 2 and do not insert into the hydrophobic core region of the membrane with the exception of the 20-residue-long G8C mutant for which the mutation creates a stable obliquely inserted configuration. The obliquely inserted configuration of the G8C-mutant is energetically comparable with the interfacial orientation. The orientations are shown in Fig. 3. The fact that the energy of the oblique

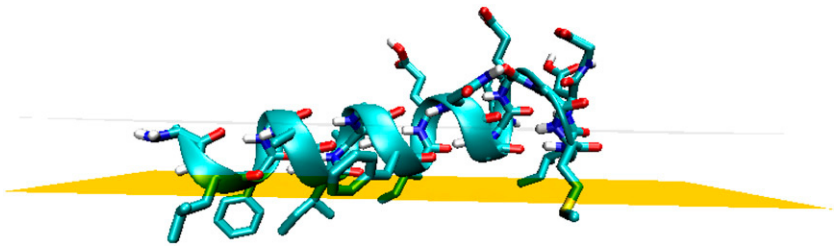

FIGURE 2 The slightly tilted orientation adopted by the hemagglutinin fusion peptide. The yellow plane represents the lipid tail-headgroup interface and the gray plane shows the level at which the lipid phosphate group is estimated to be. Although the peptide is straight and helical in this minimized structure, the dynamics of the peptide show that the peptide behaves in a hingelike fashion: The N-terminus and the C-terminus form two separate helices. In the figure, the acidic residues are uncharged. This figure, as well as Figs. 3, 8, 9, and 12, were produced with the program VMD (46), after which they were rendered and the planes added with POV-Ray.

orientation is comparable to the interfacial orientation demonstrates that the single point mutation can affect the energy landscape enough to introduce new stable configurations. In contrast to the wild-type and other mutants in which a kink is present in the dynamics of the peptides but not in the minimized structures, the obliquely inserted G8C mutant also occasionally shows a stable kink in the minimized fusion peptide structure as shown in Fig. 3.

Figs. 4 and 5 present the average effective energies, insertion depths, and angles with respect to membrane plane adopted by the fusion peptides in the simulations. For the 27-residue extended mutants an interesting phenomenon can be observed: the hydrophilic tail enhances the fluctuations of the peptide, which is visible as a larger scatter of data points in Fig. 5 than in Fig. 4. Furthermore, the N-terminal insertion angle increases in comparison to the 20-residue peptide. All the mutants of the 27-residue peptide adopt the interfacial orientation, but we observe two cases in which the mutants (D19C and A7C) fluctuate from obliquely inserted to interfacial configurations indicating an obliquely inserted local minimum. These special cases are marked in Fig. 5.

Figs. 6 and 7 show how the insertion depths of the simulated spin labels in the 5-ns-long runs compare with the measurements of Macosco et al. (17) and Han et al. (23). The plots show average insertion depths of the spin-label nitrogen atom and the error bar is the standard deviation of the nitrogen z-position. Spin labels in some mutants have several stable orientations and during the dynamics, the spin label flips back and forth between orientations. This shows as a larger standard deviation (*error bar*) in Figs. 6 and 7.

In Fig. 6, the simulated nitroxide label positions are in excellent agreement with the data of Macosco et al. (17) with the exception of the I6C mutant for which the experimental points indicate deeper membrane insertion than observed in the simulations of the spin label. Typical spin-label orientations for the I6C mutant are shown in Fig. 8 that show the spin label residing quite close to the peptide backbone. The measured data point is a few Ångstroms deeper in the

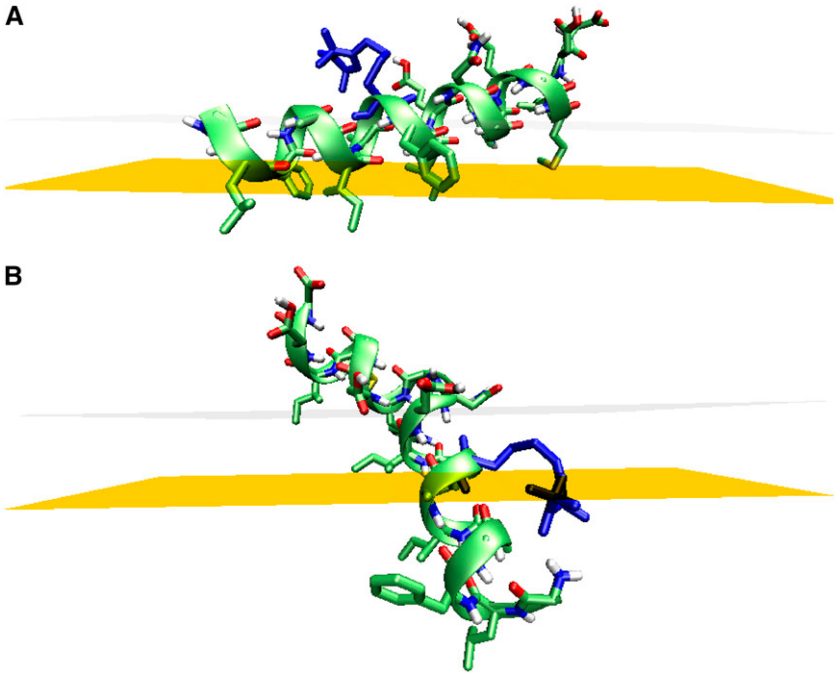

FIGURE 3 The spin-label mutation changes the energy landscape enough for a stable obliquely inserted orientation to emerge in the 20-residue-long G8C mutant. The oblique orientation is comparable in effective energy with the interfacial orientation (see Fig. 4).

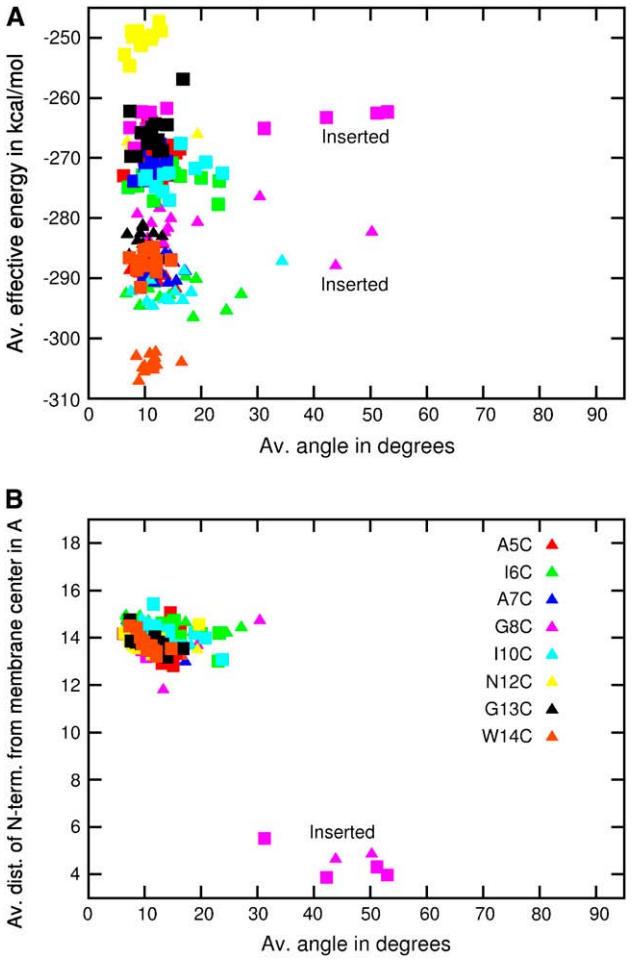

FIGURE 4 Effective energy and N-terminal insertion depth plotted against the angle with respect to the membrane plane for the spin-labeled hemagglutinin fusion peptide. Triangles refer to peptides with charged acidic residues and squares to peptides with protonated acidic residues. The energies of the states do not include the cost of (de)protonation and therefore are comparable only within the same mutant and protonation state. One of the mutants, G8C, shows a stable low-energy configuration in which the peptide adopts an oblique orientation.

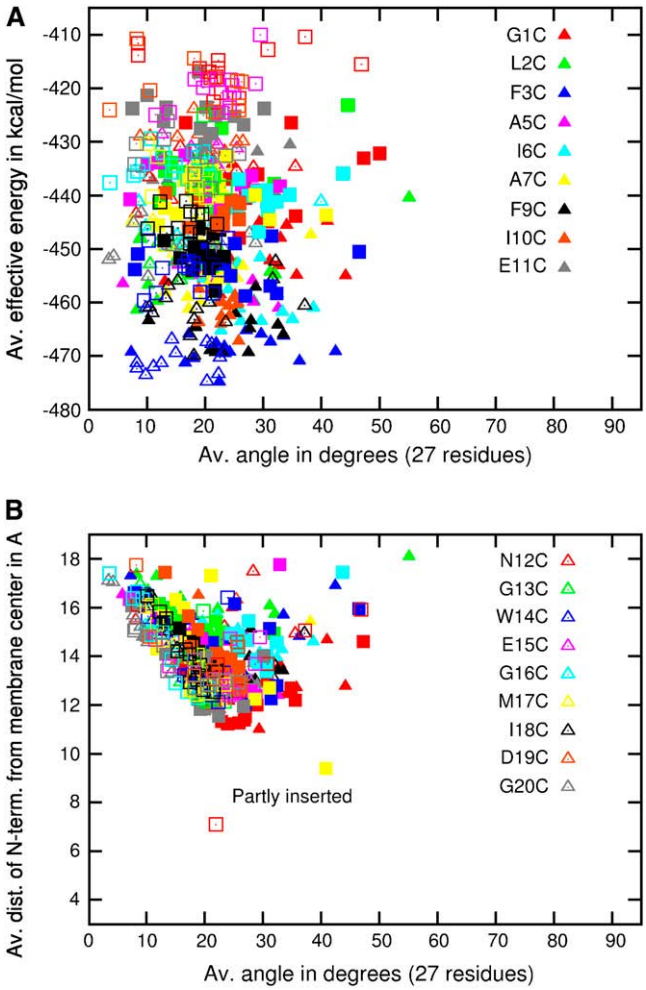

FIGURE 5 Effective energy and N-terminal insertion depth plotted against the angle with respect to the membrane plane for the spin-labeled extended 27-residue hemagglutinin fusion peptide. Triangles refer to peptides with charged acidic residues and squares to peptides with protonated acidic residues. The energies of the states do not include the cost of (de)protonation and therefore are comparable only within the same mutant and protonation state. The symbols indicating deeper membrane insertion in *B* refer to two metastable obliquely inserted mutants (A7C, D19C) that switch from oblique insertion to the interfacial configuration during the simulation.

membrane. On the other hand, spin labels at mutation site N12C extend to almost opposite directions in different configurations as shown by Fig. 9. The spin label also easily flips between the orientations, which shows as large standard deviation (*error bars*) in Fig. 6. The large standard deviation for the G8C mutant with protonated acidic residues (Fig. 6, *right side*) results from the peptide spending ~20% of the simulation in the obliquely inserted configuration and the rest in the interfacial orientation. The same mutant with charged acidic residues prefers the interfacial orientation but fluctuates more than the other mutants. The fluctuations at the W14C-mutant with charged acidic residues result from some C-terminal unwrapping of the peptide and the spin label interacting with the unsatisfied hydrogen-bonding groups of the unwrapped terminus.

The 27-residue peptide exhibits a high degree of fluctuations in the tail region. The spin label at the C-terminal half of the peptide interacts with the lysines of the tail region. This affects both the position of the spin label and its fluctuations. Often the C-terminal end of the peptide also partially unwrapped. In line with the 20-residue results, the 27-residue peptide simulation points do not reproduce the points that are deepest in the membrane, i.e., pH 5.0 L2C and F3C mutants and the W14C mutant. The spin label in the L2C and in the F3C mutants interacts with the unsatisfied hydrogen-bonding groups at the helix terminus. This is not, however, sufficient to explain the difference with experiment: if the spin label at these sites did not interact with the

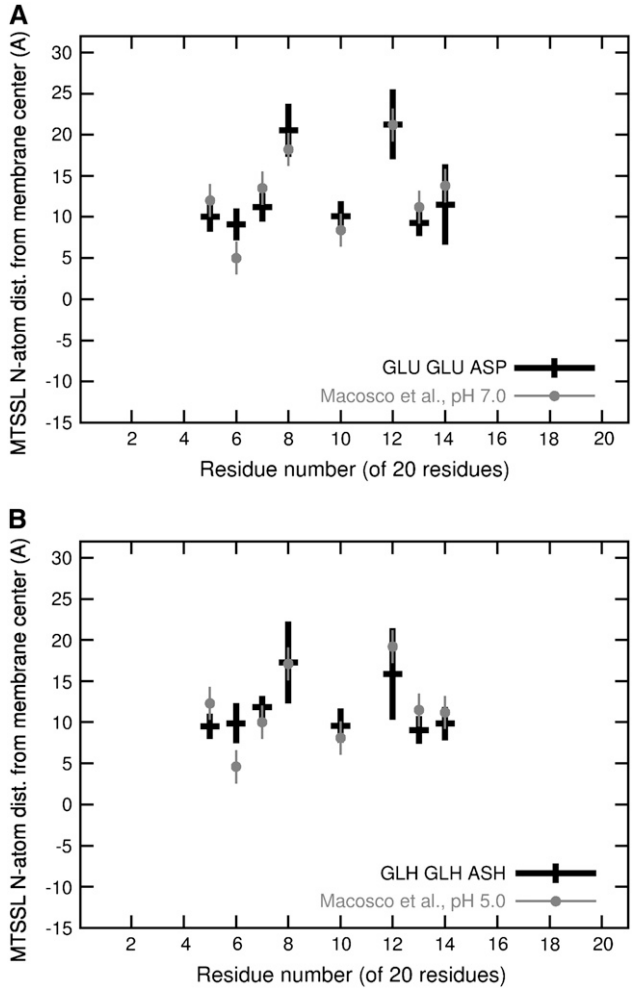

FIGURE 6 The insertion depth of MTSSL in the 20-residue peptide. The horizontal bars mark the average insertion depth of the spin-label nitrogen atom while the vertical bars show the standard deviation of the spin-label insertion depth. The error bar of experimental data of Macosco et al. (17) is estimated to be 2 Å from the graph given in that study (17). The results of Macosco et al. (17) have been converted to the coordinate system used in this work by employing the formula $d' = -d + 16.0$ Å, in which d' is plotted above and d is the insertion depth presented in Macosco et al. (17) and Han et al. (23). This coordinate transformation is necessary because we define the origin to be at the center of the membrane instead of at the lipid phosphate group level. The increment consists of our nonpolar region thickness $T/2 = 13$ Å incremented by 3 Å for the lipid phosphate headgroup.

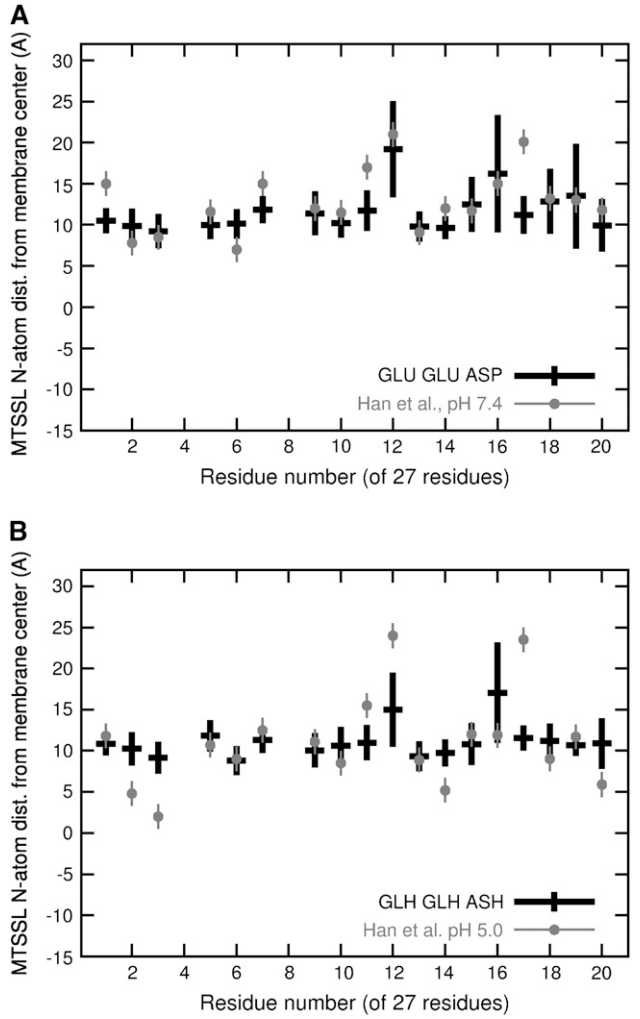

FIGURE 7 The insertion depth of MTSSL in the 27-residue extended peptide. As in Fig. 6, the horizontal bars mark the average insertion depth of the spin-label nitrogen atom while the vertical bars show the standard deviation of the spin-label insertion depth. The error bar of experimental data of Han et al. (23) was reported to be 1.5 Å in that study (23). The results of Han et al. (23) have been converted to the coordinate system analogous to Fig. 6.

N-terminus, it would be only a few Ångstroms deeper in the membrane. The spin label in the pH 5.0 W14C mutant points mostly toward the membrane center but also spends parts of the simulation pointing toward the peptide backbone—should the spin label prefer entirely the former orientation, the experimental point would be reproduced. This discrepancy in reproducing the data points corresponding to deepest insertion in the experiments is discussed later from the methodological viewpoint.

The experimental points corresponding to the 27-residue E11C mutant are somewhat above the simulation points (Fig. 7). For the E11C mutant, we see the spin label mostly pointing toward the membrane center instead of away from it, which would correspond to the experimental data points. Although our spin label is equally hydrophobic as experimentally measured (see Appendix A), the hydrophobicity calculation contains a relatively large uncertainty. This may be enough to destabilize the away-from-membrane-center orientation that we occasionally see.

As in the 20-residue peptide, the spin label in the N12C mutant shows high configurational flexibility pointing at opposite orientations. The simulation data for the N12C mutant at low pH appear to be lower than the experimental point. This could be due to a sampling deficiency of the simulation at this highly flexible site (the pH 7 simulation data cover the experimental point).

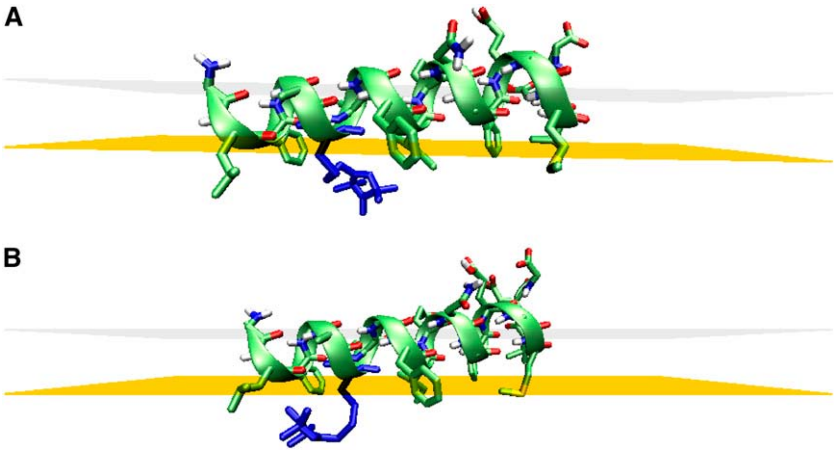

FIGURE 8 Typical spin-label orientations in the 20-residue-long I6C mutant.

The large error bars for the C-terminal mutants starting from G16C result from a variable degree of interaction with the tail lysines. This causes uncertainty in the predictions of the C-terminal spin-label position. Curiously, however, we do not observe the relatively far-from-the-membrane orientation for the M17C mutant spin label. In our simulations, the M17C spin label prefers to stay in contact with the membrane. There is some evidence that the peptide may have adopted a 3_{10}-helix structure at the C-terminal end in the experiments (23). Our peptide remains α-helical; a structural change to a 3_{10}-helix would definitely change the preferred orientations of some of the spin labels, presumably also M17C. Because of the tail interactions and occasional unwrapping of the C-terminal region, we have large standard deviations for a majority of the C-terminal mutants and cannot conclude whether the measurement points would agree more with a 3_{10}-helical backbone.

Table 1 presents the average difference in membrane insertion depth for the MTSSL nitrogen atom and the C_α-atom in the peptides, as well as the distance between the two atoms. In most mutants, the nitrogen label is significantly deeper in the membrane than the backbone C_α-atom, even for residues on the solvent side of the helix. The table also shows that the distance between the C_α-atom and the nitrogen atom in the spin label varies between 4.3 Å and 7.6 Å. The small standard deviations show that this distance, i.e., the arm length of the residue, is quite fixed within each site; the difference in insertion depth fluctuates much more. The largest fluctuations are observed for the N12C mutant for both peptide lengths, which is also visible in Figs. 6 and 7. Another ''unstable'' spin-label site is the 20-residue G8C mutant that has two competing orientations. In the C-terminal mutants, the fluctuations in depth stand out for the 27-residue E15C, G16C, I18C, and D19C mutants when the acidic residues are charged. The protonation of the acidic residues stabilizes the C-terminal half of the peptide.

Figs. 10 and 11 show the dihedral-angle probability distributions of MTSSL in peptides with charged acidic residues. The distributions show that the peaks corresponding to high probability angles may vary in position significantly between different mutation sites. Some trends can be observed: typically, the angle χ_1 has a *trans*-orientation but may also

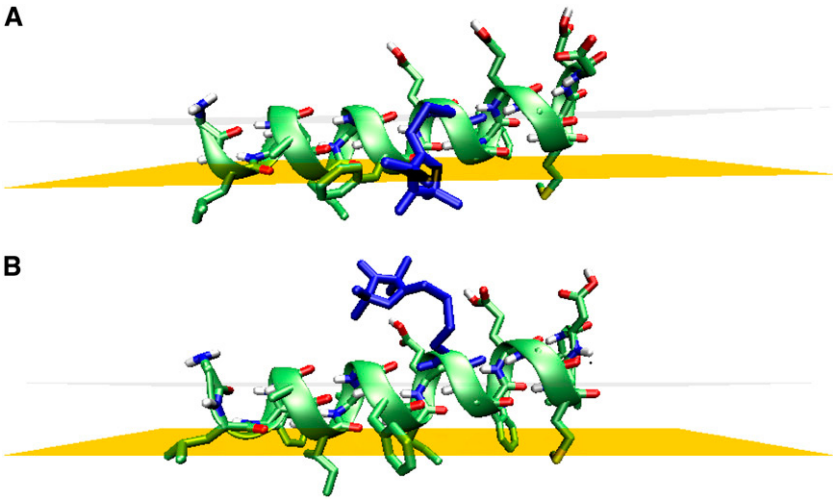

FIGURE 9 Typical spin-label orientations in the 20-residue-long N12C mutant. The N-terminus is toward the left.

TABLE 1 Relative membrane insertion $\Delta z = z_{N_{sl}} - z_{C_\alpha}$ and the spin-label distance ΔR from the corresponding C_α-atom

20-Residue Mutant	Δz (Å)	$\sigma_{z,\ 20}$ (Å)	ΔR (Å)	$\sigma_{R,\ 20}$ (Å)
A5C	−5.95 (−5.19)	1.15 (1.76)	7.47 (7.00)	0.45 (0.90)
I6C	−4.72 (−5.51)	1.57 (1.61)	6.16 (6.64)	1.09 (1.11)
A7C	−2.56 (−3.50)	1.00 (1.32)	4.98 (5.41)	0.60 (0.92)
G8C	0.19 (2.71)	3.56 (3.01)	6.55 (6.66)	0.95 (0.84)
I10C	−5.43 (−5.81)	1.87 (1.28)	7.00 (6.75)	0.96 (0.94)
N12C	−1.89 (2.40)	4.42 (3.66)	6.99 (6.73)	0.65 (0.68)
G13C	−5.94 (−6.63)	1.46 (1.39)	7.22 (7.37)	0.83 (0.93)
W14C	−5.31 (−4.50)	1.78 (3.52)	6.89 (7.18)	0.91 (0.98)
27-Residue Mutant	Δz (Å)	σ_{z27} (Å)	ΔR (Å)	$\sigma_{R,27}$ (Å)
G1C	−2.98 (−3.82)	0.95 (1.12)	4.33 (5.11)	0.30 (0.60)
L2C	−4.29 (−4.95)	1.59 (1.81)	5.38 (6.42)	1.31 (1.33)
F3C	−5.22 (−5.58)	1.84 (1.34)	6.61 (6.75)	0.82 (0.57)
A5C	−2.89 (−5.54)	1.61 (1.54)	5.71 (7.39)	0.84 (0.67)
I6C	−5.17 (−5.17)	1.45 (1.30)	6.81 (6.12)	0.78 (1.00)
A7C	−3.52 (−3.01)	1.20 (1.11)	5.34 (5.00)	0.79 (0.57)
F9C	−5.52 (−4.96)	1.83 (1.86)	7.27 (7.21)	0.85 (0.81)
I10C	−5.94 (−5.80)	1.43 (1.51)	7.15 (7.05)	0.80 (0.91)
E11C	−4.60 (−4.27)	1.46 (1.67)	6.24 (6.33)	0.77 (0.85)
N12C	−2.44 (−0.50)	3.67 (4.10)	7.01 (7.07)	0.64 (0.78)
G13C	−6.29 (−6.10)	1.61 (1.33)	7.48 (7.42)	0.71 (0.66)
W14C	−5.67 (−6.29)	1.31 (0.76)	6.91 (6.83)	0.90 (0.58)
E15C	−5.52 (−4.57)	1.48 (2.12)	6.72 (7.56)	0.39 (0.72)
G16C	−1.72 (−3.23)	4.65 (4.13)	6.76 (7.16)	1.02 (0.69)
M17C	−6.42 (−6.06)	0.91 (1.72)	7.54 (7.47)	0.61 (0.69)
I18C	−6.37 (−5.18)	1.11 (2.51)	7.27 (7.49)	0.69 (0.49)
D19C	−5.15 (−5.00)	0.94 (2.75)	5.96 (6.81)	0.86 (0.81)
G20C	−6.02 (−6.61)	1.43 (1.51)	7.18 (7.59)	0.92 (0.71)

Standard deviations σ_z and σ_R describe the fluctuations. The quantities in parentheses correspond to peptides with charged acidic residues whereas the numbers outside the parentheses correspond to peptides with neutralized acidic residues.

adopt *gauche*-orientation (*g*-) in some environments. The angle χ_2 has two preferred orientations. The distribution is also wider than in the case of χ_1. The disulfide dihedral angle χ_3 is relatively fixed at ~90° except for a couple of cases in which the distribution flips to the corresponding negative values. The angles χ_4 and χ_5 show most flexibility in their distributions. Their barriers appear to be the smallest, indicating that most fluctuations are due to these two angles in accordance with Langen et al. (20) and Columbus et al. (40). However, χ_1 and χ_2 are the major contributors in the site-dependent orientation of the residue. Figs. 8, 9, and 12 show examples of spin-label orientations at different mutation sites.

DISCUSSION

The molecular dynamics simulations reported here show that the assumptions made to simplify the analysis of spin-label-based EPR measurements have limitations. We find that the commonly used MTSSL may induce new membrane configurations for the labeled peptide. We observed one of the studied influenza hemagglutinin fusion peptide mutants, namely the 20-residue-long G8C mutant, to adopt also an obliquely inserted membrane orientation that clearly differed from the slightly tilted interfacial orientations obtained for the wild-type and the majority of the mutants. For several other mutants, we observed the obliquely inserted configuration as a local minimum upon spin-labeling. For the wild-type peptide, this minimum was not observed.

Furthermore, because MTSSL is relatively hydrophobic, a clear bias toward deeper membrane insertion than the corresponding backbone C_α-atom was observed for the spin label. On the average, the nitrogen atom in the spin label is several Ångstroms deeper in the membrane than the corresponding C_α even for sites facing the solvent. MTSSL was also observed to show site-dependent orientations and flexibility in accordance with the crystal structures of Langen et al. (20), in which several MTSSL orientations are observed depending on the site of mutation, and with Owenius et al. (28), in which the local environment is reported to change the spin-label response in a label-dependent manner. The studied MTSSL residue adopts configurations in which the difference between shortest and longest arm lengths is 3.3 Å. Considering that the arm length was observed to vary between 4.3 Å and 7.6 Å in the study, the site-to-site variance can be >30% from any sensible fixed-arm-length value.

Macosco et al. (17) and Han et al. (23) provide MTSSL-based experimental results of the membrane insertion and orientation with respect to membrane for the influenza hemagglutinin fusion peptide. From the data of Macosco et al. (17) an insertion angle of 25° (pH 7.0) or 28° (pH 5.0) was deduced while the N-terminal insertion depth was reported to be close to the phosphate headgroup level (17,26). Han et al. (23) predicted a helix-break-helix configuration in which both the N-terminus and the C-terminus insert deep into the hydrophobic core of the membrane. The N-terminal helix was reported to adopt an angle of 21 or 37° depending on pH with respect to membrane plane. Experimental studies based on methods other than MTSSL for deducing the influenza hemagglutinin fusion peptide configuration in membrane predict the peptide to adopt an α-helical form with an angle of 45° (25) or take a parallel-to-membrane orientation (27). Both studies predict an interfacial insertion depth. We observe in the simulations the peptide to adopt a slightly tilted orientation at the lipid headgroup-tail interface (30). The tilt angle of 12.4° is less than the tilt angles reported based on experiments with the exception of Dubovskii et al. (27), but in line with existing simulation studies (31–33,41–43); see also the discussion in Sammalkorpi and Lazaridis (30).

The simulations of the spin-labeled mutants show that with the exception of the I6C mutant, the spin-label positions reproduce the measurements of Macosco et al. (17). From these data, a more tilted orientation was deduced. The observed interfacial insertion depth relates well with the

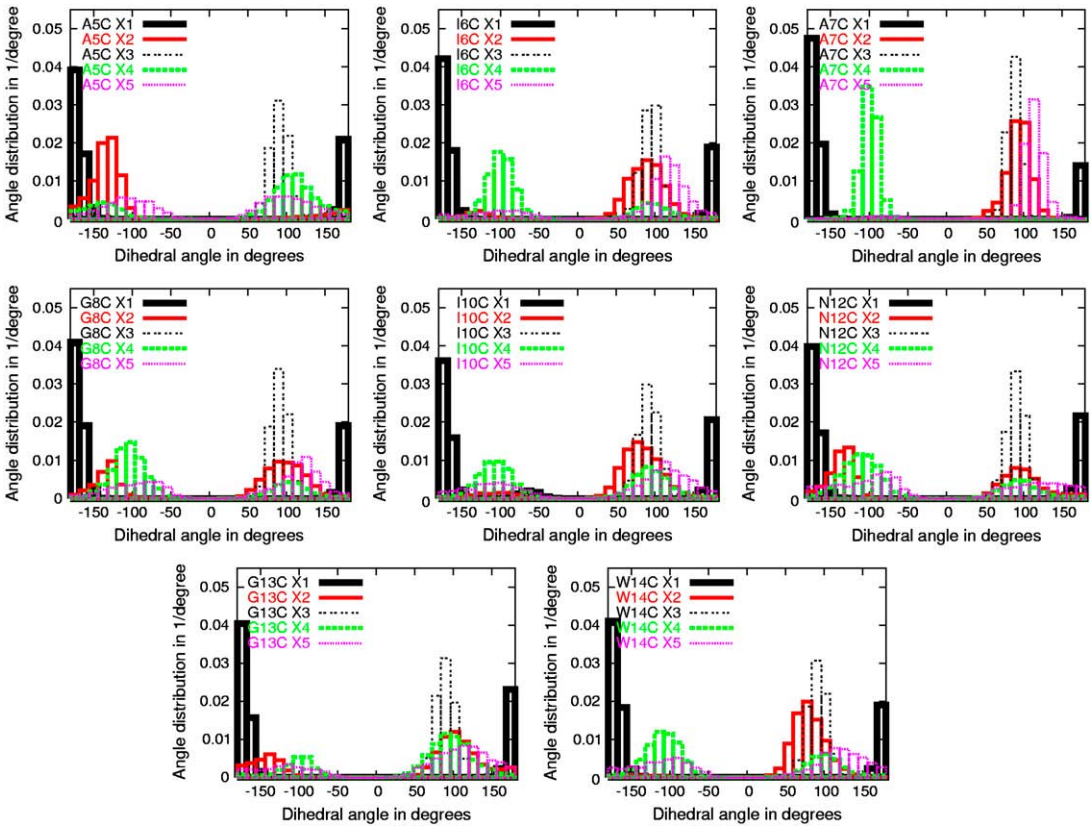

FIGURE 10 Dihedral-angle distributions of MTSSL residue at different mutation sites of the 20-residue peptide. The distributions correspond to peptides with charged acidic residues. The plotted dihedral angles are the $N-C_\alpha-C_\beta-S$ (χ_1), $C_\alpha-C_\beta-S-S$ (χ_2), $C_\beta-S-S-C$ (χ_3), $S-S-C-C$ (χ_4), and $S-C-C-C$ (χ_5) (see Fig. 1).

N-terminal insertion depth reported in Macosco et al. (17) and Zhou et al. (26). In Han et al. (23), an extended 27-residue peptide with spin-labeling also in the C-terminal half of the peptide was studied. Our simulations are able to reproduce most of the measurement data points of Han et al. (23), based on which the V-shaped structure with both termini deep in the hydrophobic core of the membrane was reported. However, the experimental data points of some residues, namely the most deeply inserted pH 5.0 L2C, F3C, and W14C are not reproduced, as well as the E11C and M17C mutants at both pH values. Some of the deep insertion experimental data points, i.e., I6C in the 20-residue peptide and the W14C in the 27-residue peptide, would be possible to reproduce with a more extended spin-label conformation, without a change in helix orientation. Other points, however, such as the N-terminal mutants L2C and F3C at pH 5.0 in the 27-residue peptide, seem to require a more oblique orientation or deeper membrane insertion of the helix.

The inability to reproduce the deepest spin-label points may be due to the limitations of the implicit membrane model. IMM1 is a highly simplified model of a lipid bilayer and assumes a perfectly flat, nondeformable membrane. Lagüe et al. (43), in which the membrane is described explicitly in the simulation, shows the lipids making room for the peptide and creating a crevice in the membrane upon the fusion peptide binding. This crevice may be enough to enable the spin label to insert deeper into the membrane when the residue is oriented toward the membrane-center. The IMM1 description is unable to reproduce the opening of a crevice, which may contribute to the failure to reproduce the deeply inserted spin-label position. Alternatively, there may be caveats with the experimental approach. The polarity gradient assumed by the collision gradient method (24) may be affected by the presence of a peptide adsorbed on the membrane surface. For example, hydrophobic peptide side chains may affect the distribution of O_2 in the membrane. In addition, steric hindrance by the peptide may affect access of the polar NiEDDA to the spin label so that the latter will appear deeper than it really is.

Although there is some support for the kinked structure (41–44), the spin-label depth profile at the C-terminal end in Han et al. (23) can also be explained by the flexibility of the MTSSL with the exception of the M17C mutant. For the M17C mutant, the reason for not reproducing the experimental data point may lie in the prediction of Han et al. (23) that the C-terminal part of the peptide would form a short 3_{10}-helix. As we employ an initially α-helical structure, we might overlook the potential transformation to a 3_{10}-helix. It

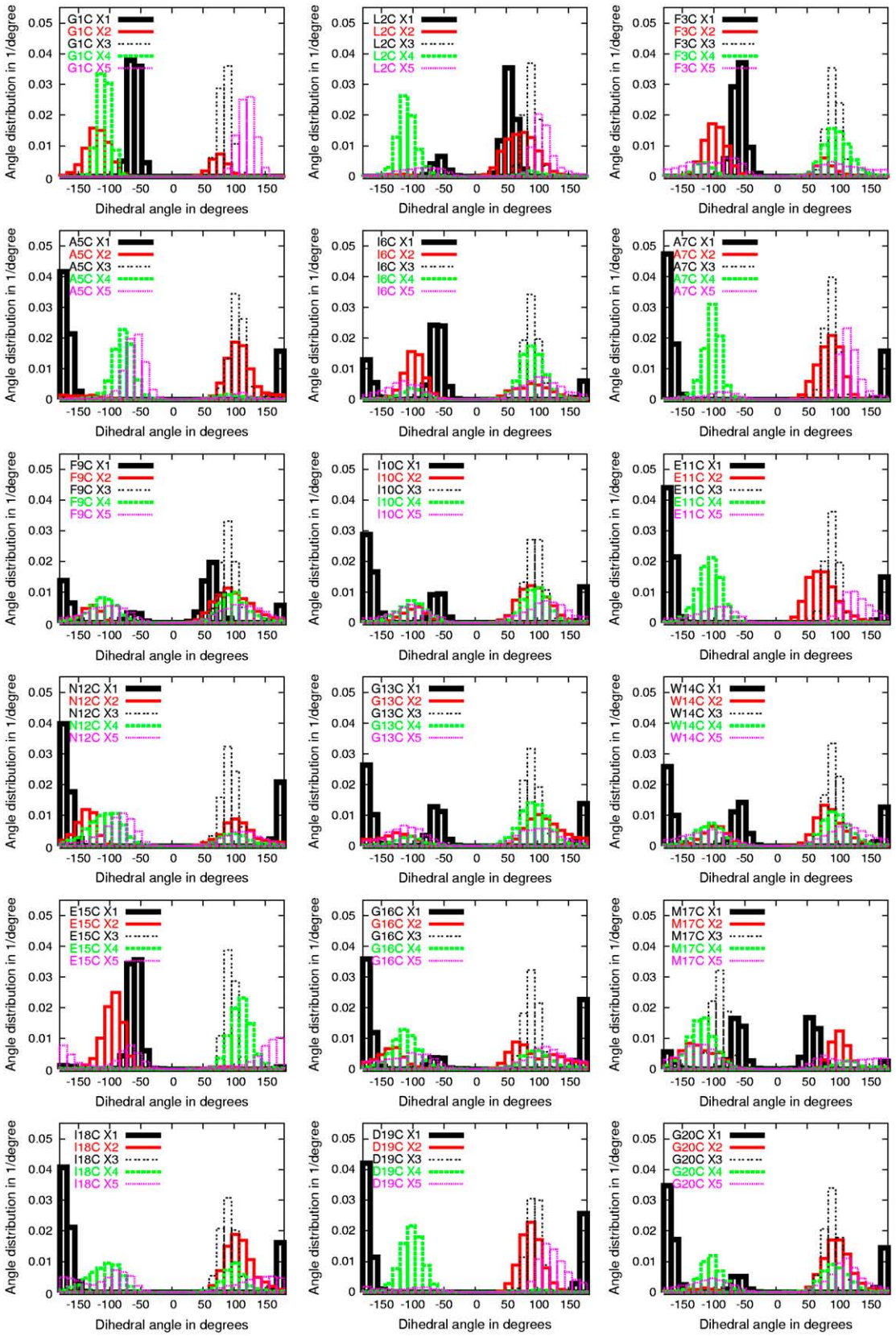

FIGURE 11 Dihedral-angle distributions of MTSSL residue at different mutation sites of the 27-residue peptide. The distributions correspond to peptides with charged acidic residues. The plotted dihedral angles are the $N-C_\alpha-C_\beta-S\,(\chi_1)$, $C_\alpha-C_\beta-S-S\,(\chi_2)$, $C_\beta-S-S-C\,(\chi_3)$, $S-S-C-C\,(\chi_4)$, and $S-C-C-C\,(\chi_5)$ (see Fig. 1).

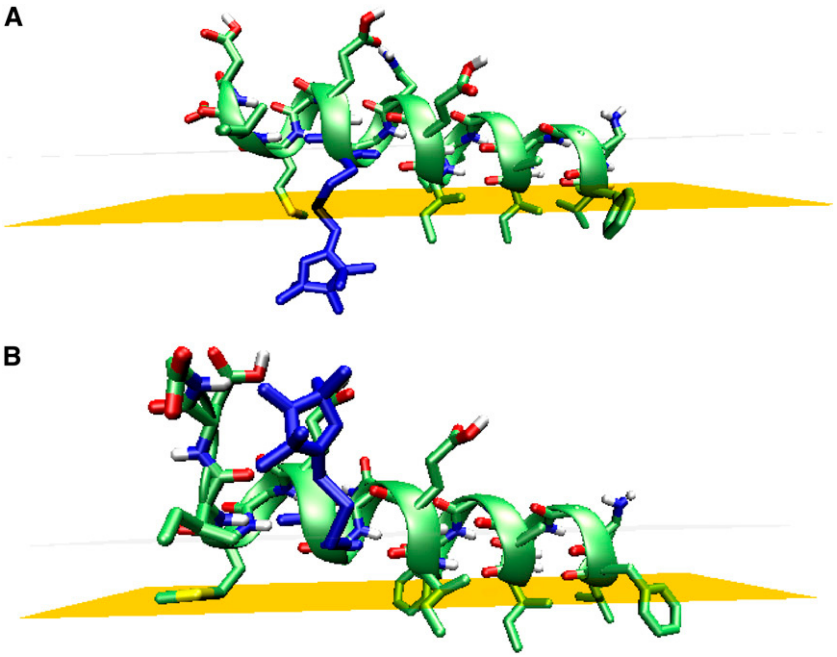

FIGURE 12 Typical spin-label orientations in the 20-residue-long W14C mutant. The N-terminus is toward the right. The second figure shows that the spin-label may also interact with the terminus, although the configuration presented above is more typical.

should be noted that, in our force field, α-helices are significantly more stable than 3_{10} helices.

The timescale of the simulations (5 ns) seems short compared to the experimental timescales. It should be noted, however, that the true timescale of implicit solvent simulations is at least an order-of-magnitude longer than the nominal time due to absence of solvent friction. Still, the high flexibility of the spin label for some mutants led to relatively large error bars in the average position of the label, which indicates that the distribution of the label is not fully converged. These spin-label position fluctuations are probably fast compared to the timescale of the EPR experiment so that the measured positions correspond to averages.

We conclude that MTSSL has a clear hydrophobic insertion bias; it exhibits a high degree of site-dependent flexibility; and the spin-labeling may induce new configurations for the labeled peptide. Although the observed spin-labeling induced configurations in which the labeled peptide inserted into the membrane may be local minima, their emergence indicates that care should be exercised when assuming that the spin-labeling does not change the configuration of the labeled peptide. Especially short, amphiphilic peptides may undergo such configurational changes upon spin-labeling and membrane interaction. Furthermore, the flexibility and site-dependent orientations of the spin label should be taken

TABLE 2 CHARMM parameters for the MTSSL residue: parameters for the bond-energy function $\frac{1}{2}k_b(b - b_0)^2$

Type	Type	$\frac{1}{2}k_b$ Kcal mol^{-1} Å^{-2}	b_0 Å	Source
NO	*CR*	350.0	1.502	(45)
NO	*ON*	520.0	1.277	(45)
CR	*CR*	450.0	1.38	Adopted *C–C* from (35)
CR	*CR1E*	450.0	1.38	Adopted *C–CR1E* from (35)
CR	*CH2E*	405.0	1.52	Adopted *C–CH2E* from (35)
CR	*CH3E*	405.0	1.52	Adopted *C–CH3E* from (35)
CH2E	*S*	450.0	1.81	Adopted *CH2E–SH1E* from (35)
S	*S*	500.0	2.02	Adopted *SH1E–SH1E* from (35)

TABLE 3 CHARMM parameters for the MTSSL residue: parameters for the bond-angle energy function $\frac{1}{2}k_\theta(\theta - \theta_0)^2$

Type	Type	Type	$\frac{1}{2}k_\theta$ Kcal mol^{-1}	θ_0 Degrees	Source
CR	*CR*	*NO*	20.0	109.45	(45)
CR	*NO*	*CR*	24.0	124.0	(45)
CR	*NO*	*ON*	73.0	118.0	(45)
CR	*CR1E*	*CR*	70.0	122.5	Adopted *C–C–CR1E* from (35)
CR1E	*CR*	*CH3E*	70.0	106.5	Adopted *C–C–C* or *C–CH1E–CH3E* from (35)
CH3E	*CR*	*CH3E*	70.0	106.5	Adopted *C–C–C* or *C–CH1E–CH3E* from (35)
CR	*CR*	*CH3E*	70.0	122.5	Adopted *C–C–CR1E* from (35)
CR	*CR*	*NO*	20.0	109.45	(45)
CR1E	*CR*	*NO*	20.0	109.45	Adopted *CR-CR-NO* from (45)
CH3E	*CR*	*NO*	20.0	109.45	Adopted *CR-CR-NO* from (45)
S	*CH2E*	*CR*	50.0	112.5	Adopted *CH–CH2 SH1E* from (35)
CH2E	*S*	*S*	50.0	104.2	Adopted *CH2E–SH1E–SH1E* (35)
CH2E	*CR*	*CR1E*	70.0	121.5	Adopted *CH2E–C–CR1E* from (35)
CR	*CR*	*CH2E*	65.0	126.5	Adopted *C–C–CH2E* from (35)

TABLE 4 CHARMM parameters for the MTSSL residue: parameters for the dihedral angle energy function $\frac{1}{2}k_\phi[1+\cos(n\phi-\delta)]$

Type	Type	Type	Type	½k_ω Kcal/mol	n	δ Degrees	Source
CR	*CR*	*NO*	*ON*	0.118	3	0.0	(45)
CR1E	*CR*	*NO*	*ON*	0.118	3	0.0	Adopted *C–C–NO–ON* from (45)
CH3E	*CR*	*NO*	*ON*	0.118	3	0.0	Adopted *C–C–NO–ON* from (45)
CR	*CR*	*NO*	*CR*	0.118	3	0.0	(45)
CR1E	*CR*	*NO*	*CR*	0.118	3	0.0	Adopted *C–C–NO–C* from (45)
CH3E	*CR*	*NO*	*CR*	0.118	3	0.0	Adopted *C–C–NO–C* from (45)
CR1E	*CR*	*CR*	*NO*	0.158	3	0.0	(45)
CR	*CR1E*	*CR*	*NO*	0.158	3	0.0	Adopted *C–C–C–NO* from (45)
CH2E	*CR*	*CR*	*NO*	0.158	3	0.0	Adopted *C–C–C–NO* from (45)
CH2E	*CR*	*CR*	*CH3E*	5.0	2	180.0	Adopted *C–CR–CR–C* from (35)
CR1E	*CR*	*CR*	*CH3E*	5.0	2	180.0	Adopted *C–CR–CR–C* from (35)
CH2E	*CR*	*CR*	*CR1E*	5.0	2	180.0	Adopted *C–CR–CR–C* from (35)
CH2E	*CR*	*CR*	*CR*	5.0	2	180.0	Adopted *C–CR–CR–C* from (35)
CH2E	*CR*	*CR1E*	*CR*	5.0	2	180.0	Adopted *C–CR–CR–C* from (35)
X	*CR*	*CR1E*	*X*	0.0	3	0.0	Adopted *X–C–CH–X* from (35)
X	*CR1E*	*CR1E*	*X*	1.6	3	0.0	Adopted *X–CH–CH–X* from (35)

into account as potential sources of error. Perhaps the accuracy of spin-label-based EPR measurements could be improved by combining modeling to measurements as done in Baumann et al. (21) or by performing the measurements using two different spin labels and knowledge of the physical properties of each label.

APPENDIX A: A PARAMETRIZATION OF THE NITROXIDE SPIN LABEL

The CHARMM 19 force field (35) and the IMM1 environment description (36,37) do not contain parameters for the MTSSL. The necessary force constant parameters for the nitroxide group were obtained from Morelon et al. (45), where the parameters for a similar nitroxide label were derived based on ab initio calculations. The carbon-carbon parameters were deduced from analogous existing parameters (35). The necessary partial charges for the nitroxide group were obtained from Morelon et al. (45), and the resulting charge is neutralized by the two sp^3-coordinated carbon atoms neighboring the nitrogen, *NO*. The employed CHARMM parameter values for this nitroxide label are shown in Tables 2–5. In the tables, the atom types are referred to in the same way as in the CHARMM program. The atom type *CR* is identical to atom type *C* except for IMM1 solvation parameters that are presented in Lazaridis (36).

TABLE 5 CHARMM parameters for the MTSSL residue: parameters for the improper dihedral energy function $\frac{1}{2}k_\omega(\omega-\omega_0)^2$

Type	Type	Type	Type	½k_ω Kcal/mol rad^2	ω_0 Degrees	Source
CR	*CR1E*	*CR*	*CH2E*	90.0	0.0	Adopted *C–CR1E–C–CH2E* from (35)
CR	*X*	*X*	*CR*	25.0	0.0	Adopted *CR1E–X–X–CR1E* from (35)
CR	*X*	*X*	*CR1E*	25.0	0.0	Adopted *CR1E–X–X–CR1E* from (35)
CR	*X*	*X*	*CH3E*	25.0	0.0	Adopted *C–X–X –CH3E* from (35)
NO	*X*	*X*	*CR*	25.0	0.0	Adopted *NR–X–X–C* from (35)
NO	*X*	*X*	*ON*	25.0	0.0	Approximated based on existing (35) nitrogen and oxygen parameters

The improper torsion angle ω is defined for a set of particles (*A*,*B*,*C*,*D*) as the angle between the planes *ABC* and *BCD*.

IMM1 solvation parameters of the proline nitrogen have been used for the nitrogen atom in the nitroxide label, *NO*. In the membrane environment the nitroxide oxygen *ON* shares the solvation parameters of the carbonyl oxygen. However, the oxygen in the spin label is significantly less polar. Therefore, the *ON* solvation parameters in water were decreased by 20% from those of the carbonyl oxygen. To assess the accuracy of this estimated reduction we compared the hydrophobicity of the MTSSL residue and LEU residue. The hydrophobicity was computed as the effective energy difference of a single residue in water and at the water-membrane interface with the side chain embedded into the nonpolar membrane environment. The residue was first placed at the hydrophobic-hydrophilic interface, relaxed for 100 ps at 300 K, and then minimized by using the adopted basis Newton-Raphson method (34). This was repeated for different initial velocity assignments and the average effective energy of 20 relaxed and minimized structures was used as the effective energy of the residue at the interface or in water. For the LEU residue, the effective energy difference calculated in this way was 1.97 ± 0.85 kcal/mol in favor of the interfacial position whereas for the MTSSL residue we obtained a difference of 2.70 ± 0.89 kcal/mol also in favor of the interfacial position. The error has been estimated by the standard deviation of the effective energy values. That is, we found that the MTSSL

TABLE 6 The parameters required for the nitroxide spin label in the solvation model

	Volume Å^3	G^{ref} Kcal/mol	G^{free} Kcal/mol	H^{ref} Kcal/mol	C_P^{ref} cal/mol
NO_{H_2O}	4.4	−1.000	−1.550	−1.250	8.80
NO_{chex}	4.4	−1.145	−1.720	−1.843	0.00
ON_{H_2O}	10.8	−4.337	−4.740	−4.687	−7.13
ON_{chex}	10.8	−1.270	−1.390	−2.045	0.00

For the nitrogen, the solvation parameters of proline nitrogen have been adopted. The oxygen atom in the label is otherwise analogous to carbonyl oxygen but less polar. This has been taken into account by reducing the magnitude of the solvation parameters by 20% in water. The original proline nitrogen and the carbonyl parameterization is presented in Lazaridis (36).

residue is 0.73 ± 1.2 kcal/mol more hydrophobic than a leucine residue, which compares well with the 0.7 kcal/mol difference reported in Yu et al. (29), although there is a substantial statistical uncertainty. The solvation parameters that differ from those published in Lazaridis (36) are presented in Table 6.

M.S. thanks M. Koivunen for fruitful scientific discussions.

Financial support was provided by National Institutes of Health SCORE grant No. 3S06GM008168-25S1. Infrastructure support was provided in part by grant No. RR03060 from the National Institutes of Health.

REFERENCES

1. Hubbell, W. L., and C. Altenbach. 1994. Investigation of structure and dynamics in membrane-proteins using site-directed spin labeling. *Curr. Opin. Struct. Biol.* 4:566–573.
2. Hubbell, W. L., A. Gross, R. Langen, and M. A. Lietzov. 1998. Recent advances in site-directed spin labeling of proteins. *Curr. Opin. Struct. Biol.* 8:649–656.
3. Borbat, P. P., A. J. Costa-Filho, K. A. Earle, J. K. Moscicki, and J. H. Freed. 2001. Electron spin resonance in studies of membranes and proteins. *Science.* 291:266–269.
4. Möbius, K., A. Savitsky, C. Wegener, M. Plato, M. Fuchs, A. Schnegg, A. A. Dubinskii, Y. A. Grishin, I. A. Grigor'ev, M. Kühn, D. Duché, H. Zimmermann, and H.-J. Steinhoff. 2005. Combining high-field EPR with site-directed spin-labeling reveals unique information on proteins in action. *Magn. Reson. Chem.* 43:S4–S19.
5. Hubbell, W. L., H. S. Mchaourab, C. Altenbach, and M. A. Lietzov. 1996. Watching proteins move using site-directed spin-labeling. *Structure.* 4:779–783.
6. Hubbell, W. L., S. Cafiso, and C. Altenbach. 2000. Identifying conformational changes with site-directed spin-labeling. *Nat. Struct. Biol.* 7:735–739.
7. Columbus, L., and W. L. Hubbell. 2002. A new spin on protein dynamics. *Trends Biochem. Sci.* 27:288–295.
8. Malmberg, N. J., and J. J. Falke. 2005. Use of EPR power saturation to analyze the membrane-docking geometries of peripheral proteins: applications to C2 domains. *Annu. Rev. Biophys. Biomol. Struct.* 34: 71–90.
9. Fajer, P. G. 2000. Electron spin resonance spectroscopy labeling in peptide and protein analysis. *In* Encyclopedia of Analytical Chemistry. John Wiley Sons, Chichester, UK.
10. Thorgeirsson, T. E., W. Xiao, L. S. Brown, R. Needleman, J. K. Lanyi, and Y.-K. Shin. 1997. Transient channel-opening in bacteriorhodopsin: an EPR study. *J. Mol. Biol.* 273:951–957.
11. Perozo, E., D. M. Cortes, and L. G. Cuello. 1998. Three-dimensional architecture and gating mechanism of a K^+ channel studied by EPR spectroscopy. *Nat. Struct. Biol.* 5:459–469.
12. Liu, Y. S., P. Sompornpisut, and E. Perozo. 2001. Structure of the KcsA channel intracellular gate in the open state. *Nat. Struct. Biol.* 8: 883–887.
13. Merianos, H. J., N. Cadieux, C. H. Lin, R. J. Kadner, and D. S. Cafiso. 2000. Substrate-induced exposure of an energy-coupling motif of a membrane transporter. *Nat. Struct. Biol.* 7:205–209.
14. Mchaourab, H. S., M. A. Lietzov, K. Hideg, and W. L. Hubbell. 1996. Motion of spin-labeled side chains in T4 lysozyme. Correlation with protein structure and dynamics. *Biochemistry.* 35:7692–7704.
15. Lietzow, M. A., and W. L. Hubbell. 2004. Motion of spin-label side chains in cellular retinol-binding protein: correlation with structure and nearest-neighbor interactions in an ant parallel β-sheet. *Biochemistry.* 43:3137–3151.
16. Cornea, R. L., L. R. Jones, J. M. Autry, and D. D. Thomas. 1997. Mutation and phosphorylation change the oligomeric structure of phospholamban in lipid bilayers. *Biochemistry.* 36:2960–2967.
17. Macosco, J. C., C.-H. Kim, and Y.-K. Shin. 1997. The membrane topology of the fusion peptide region of influenza hemagglutinin determined by spin-labeling EPR. *J. Mol. Biol.* 267:1139–1148.
18. Pfeiffer, M., T. Rink, K. Gerwert, D. Oesterhelt, and H.-J. Steinhoff. 1999. Site-directed spin-labeling reveals the orientation of the amino acid side-chains in the E-F loop of bacteriorhodopsin. *J. Mol. Biol.* 287:163–171.
19. Frazier, A. A., C. R. Roller, J. J. Havelka, A. Hinderliter, and D. S. Cafiso. 2003. Membrane-bound orientation and position of the synaptotagmin I C2A domain by site-directed spin-labeling. *Biochemistry.* 42:96–105.
20. Langen, R., K. J. Oh, D. Cascio, and W. L. Hubbell. 2000. Crystal structure of spin-labeled T4 lysozyme mutants: implications for the interpretation of EPR spectra in terms of structure. *Biochemistry.* 39: 8396–8405.
21. Baumann, B. A. J., H. Liang, K. Sale, B. D. Hambly, and P. G. Fajer. 2004. Myosin regulatory domain orientation in skeletal muscle fibers: application of novel electron paramagnetic resonance spectral decomposition and molecular modeling methods. *Biophys. J.* 86:3030–3041.
22. LaConte, L. E. W., V. Voelz, W. Nelson, M. Entz, and D. D. Thomas. 2002. Molecular dynamics simulation of site-directed spin-labeling: experimental validation in muscle fibers. *Biophys. J.* 83:1854–1866.
23. Han, X., J. H. Bushweller, D. S. Cafiso, and L. K. Tamm. 2001. Membrane structure and fusion-triggering conformational change of the fusion domain from influenza hemagglutinin. *Nat. Struct. Biol.* 8:715–720.
24. Altenbach, C., D. A. Greenhalgh, H. G. Khorana, and W. L. Hubbell. 1994. A collision gradient method to determine the immersion depth of nitroxides in lipid bilayers: application to spin-labeled mutants of bacteriorhodopsin. *Proc. Natl. Acad. Sci. USA.* 91:1667–1671.
25. Lüneberg, J., I. Martin, F. Nüssler, J.-M. Ruysschaert, and A. Herrmann. 1995. Structure and topology of the influenza virus fusion peptide in lipid bilayers. *J. Biol. Chem.* 270:27606–27614.
26. Zhou, Z., J. C. Macosco, D. W. Hughes, B. G. Sayer, J. Hawes, and R. M. Epand. 2000. 15N NMR study of the ionization properties of the influenza virus fusion peptide in Zwitterionic phospholipid dispersions. *Biophys. J.* 78:2418–2425.
27. Dubovskii, V., H. Li, S. Takahashi, A. S. Arseniev, and K. Akasaka. 2000. Structure of an analog of fusion peptide from hemagglutinin. *Protein Sci.* 9:786–798.
28. Owenius, R., M. Österlund, M. Lindgren, M. Svensson, O. H. Olsen, E. Persson, P.-O. Freskgard, and U. Carlsson. 1999. Properties of spin and fluorescent labels at receptor-ligand interface. *Biophys. J.* 77:2237–2250.
29. Yu, Y. G., T. E. Thorgeirsson, and Y. K. Shin. 1994. Topology of an amphiphilic mitochondrial signal sequence in the membrane-inserted state: a spin-labeling study. *Biochemistry.* 33:14221–14226.
30. Sammalkorpi, M., and T. Lazaridis. 2006. Configuration of influenza hemagglutinin fusion peptide monomers and oligomers in membranes. Accepted for publication. *Biochim. Biophys. Acta Biomembr.*
31. Efremov, R. G., D. E. Nolde, P. E. Volynsky, A. A. Chernyavsky, P. V. Dubovskii, and A. S. Arseniev. 1999. Factors important for fusogenic activity of peptides: molecular modeling study of analogs of fusion peptide of influenza virus hemagglutinin. *FEBS Lett.* 462:205–210.
32. Bechor, D., and N. Ben-Tal. 2001. Implicit solvent model studies of the interactions of the influenza hemagglutinin fusion peptide with lipid bilayers. *Biophys. J.* 80:644–655.
33. Spassov, V. Z., L. Yan, and S. Szalma. 2002. Introducing an implicit membrane in Generalized Born/solvent accessibility continuum solvent models. *J. Phys. Chem. B.* 106:8726–8738.
34. Brooks, B. R., R. E. Bruccoleri, B. D. Olafson, D. J. States, S. Swaminathan, and M. Karplus. 1983. CHARMM: a program for macromolecular energy, minimization, and dynamics calculations. *J. Comput. Chem.* 4:187–217.
35. Neria, E., S. Fischer, and M. Karplus. 1996. Simulation of activation free energies in molecular systems. *J. Chem. Phys.* 105:1902–1921.
36. Lazaridis, T. 2003. Effective energy function for proteins in lipid membranes. *Proteins.* 52:176–192.

37. Lazaridis, T., and M. Karplus. 1999. Effective energy function for proteins in solution. *Proteins*. 35:133–152.

38. Nosé, S. 1984. A unified formulation of the constant temperature molecular dynamics methods. *J. Chem. Phys.* 81:511–519.

39. Hoover, W. G. 1984. Canonical dynamics: equilibrium phase-space distributions. *Phys. Rev. A.* 31:1695–1697.

40. Columbus, L., T. Kálai, J. Jekö, K. Hideg, and W. L. Hubbell. 2001. Molecular motion of spin-labeled side chains in α-helices: analysis by variation of side chain structure. *Biochemistry.* 40:3828–3846.

41. Huang, Q., C.-L. Chen, and A. Herrmann. 2004. Bilayer conformation of fusion peptide of influenza virus hemagglutinin: a molecular dynamics study. *Biophys. J.* 87:14–22.

42. Vaccaro, L., K. J. Cross, J. Kleinjung, S. K. Straus, D. J. Thomas, S. A. Wharton, J. J. Skehel, and F. Fraternali. 2005. Plasticity of influenza haemagglutinin fusion peptides and their interaction with lipid bilayers. *Biophys. J.* 88:25–36.

43. Lagüe, P., B. Roux, and R. W. Pastor. 2005. Molecular dynamics simulations of the influenza hemagglutinin fusion peptide in micelles and bilayers: conformational analysis of peptides and lipids. *J. Mol. Biol.* 354:1129–1141.

44. Hsu, C.-H., S.-H. Wu, D.-K. Chang, and C. Chen. 2002. Structural characterizations of fusion peptide analogs of influenza virus hemagglutinin. *J. Biol. Chem.* 277:22725–22733.

45. Morelon, N.-D., G. R. Kneller, M. Ferrand, A. Grand, J. C. Smith, and M. Berc. 1998. Dynamics of alkane chains included in an organic matrix: molecular dynamics simulation and comparison with neutron scattering experiment. *J. Chem. Phys.* 109:2883–2894.

46. Humphrey, W., A. Dalke, and K. Schulten. 1996. VMD—visual molecular dynamics. *J. Mol. Graph.* 14:33–38.